

# The low-spin ground state of the giant Mn wheels

Roman Rausch and Christoph Karrasch

*Technische Universität Braunschweig, Institut für Mathematische Physik,  
Mendelssohnstraße 3, 38106 Braunschweig, Germany*

The single-molecule magnets (SMMs)  $\{\text{Mn}_{70}\}$  and  $\{\text{Mn}_{84}\}$  are characterized by a 14-site unit cell with  $S = 2$  spin sites, arranged in a circular geometry. Experimentally, these SMMs exhibit a magnetic ground state with a notably low total spin,  $S_{\text{tot}} = 5 - 7$ . This low-spin ground state has been up to now difficult to describe theoretically due to the complexity of the quantum Heisenberg model for this large system. In this work, we are in fact able to quantitatively reproduce the low-spin energy minimum by employing large-scale  $\text{SU}(2)$ -symmetric density-matrix renormalization group (DMRG) calculations using previously published exchange parameters obtained by density-functional theory. We do not find a low-spin state for the same parameters and  $S = 1$ , which leads us to propose that frustrated systems with  $S \geq 2$  are inherently prone to weak ferromagnetic interactions. This could account for the prevalence of similar low-spin Mn-based SMMs. Finally, by computing the full magnetization curve, we find wide plateaus at  $10/14$ ,  $11/14$ ,  $12/14$  and  $13/14$  of the saturation. This can be explained by independent 3-site clusters with broken inter-cluster bonds.

## I. INTRODUCTION

Recent decades saw significant advances in creating large magnetic aggregates [1], which have evolved beyond zero-dimensional molecules, and can now often be considered as finite but large condensed-matter systems. A particular highlight is the family of Mn wheel molecules, which have a unit cell of  $L_{\text{cell}} = 14$  magnetic centres (see Fig. 1) arranged on a ring. The spin sites are  $\text{Mn}^{3+}$  ions with  $S = 2$ . The successfully synthesized variants are  $\{\text{Mn}_{70}\}$  [2] and  $\{\text{Mn}_{84}\}$  [1, 3] (with  $N_{\text{cells}} = 5, 6$  and  $L = L_{\text{cell}} \cdot N_{\text{cells}}$ ). The variants  $\{\text{Mn}_{56}\}$  and  $\{\text{Mn}_{98}\}$  ( $N_{\text{cells}} = 4, 7$ ) might also be fabricable [2]. The  $\{\text{Mn}_{84}\}$  wheel has set the record as the largest single-molecule magnet (SMM) [1]. Despite the SMM classification, it actually has a relatively small ground-state spin of  $S_{\text{tot}} = 6$  ( $S_{\text{tot}}/L \approx 0.07$ ,  $S_{\text{tot}}/S_{\text{max}} \approx 0.04$ ). Similarly,  $S_{\text{tot}} = 5-8$  ( $S_{\text{tot}}/L \approx 0.07-0.11$ ,  $S_{\text{tot}}/S_{\text{max}} \approx 0.04-0.06$ ) is found for  $\{\text{Mn}_{70}\}$  [2], depending on the experimental extraction procedure and the precise chemical environment. In fact, such a low-spin state is quite typical among Mn-based SMMs. Reported compounds are listed in Tab. I.

In the absence of anisotropies, localized spins are described by the isotropic Heisenberg model

$$H = \sum_{ij} J_{ij} \mathbf{S}_i \cdot \mathbf{S}_j - g\mu_B B \sum_i S_i^z, \quad (1)$$

where  $\mathbf{S}_i = (S_i^x, S_i^y, S_i^z)$  is the vector of spin operators at site  $i$ ,  $g$  is the gyromagnetic ratio,  $\mu_B$  is the Bohr magneton, and  $B$  is the external field. For a system of  $L$  spins, the interactions are defined by the  $L \times L$  matrix  $J_{ij}$ . For  $B = 0$  the system has  $\text{SU}(2)$  invariance and the total spin

$$\left\langle \sum_{ij} \mathbf{S}_i \cdot \mathbf{S}_j \right\rangle = \langle \mathbf{S}_{\text{tot}}^2 \rangle = S_{\text{tot}}(S_{\text{tot}} + 1) \quad (2)$$

is a conserved quantity. The total magnetization is given

by

$$M_{\text{tot}} = \left\langle \sum_i S_i^z \right\rangle \quad (3)$$

and is a conserved quantity in the presence of the B-field.

The theoretical description of large molecules where the number of sites approaches  $L \sim 100$  poses a challenge to theory. Twenty years ago, the benchmark of theory-experiment comparison was set by  $\text{Mn}_{12}\text{Ac}$  (4 sites with  $S = 3/2$  and 8 sites with  $S = 2$ ), whose Hilbert space size is  $\sim 8.6 \cdot 10^6$  in the  $M_{\text{tot}} = 0$  subspace [10–12]. This is amenable to Lanczos diagonalization, so that an extensive comparison with the experiment could be carried out and the family of these systems was even termed the “drosophila of single-molecule magnetism” [13]. This approach runs into problems in the case of  $\{\text{Mn}_{84}\}$ , whose Hilbert space size is  $\sim 1.6 \cdot 10^{57}$  for  $M_{\text{tot}} = 0$ , so that no theoretical progress could be made.

Renewed interest in the  $\{\text{Mn}_{84}\}$  wheel from theory came 16 years after its original discovery [14, 15]: In a pioneering work, density-functional theory (DFT) was used to compute the 3 dominant exchange integrals and the system was treated in a simplified form [14]: The ground state of the  $\{\text{Mn}_7\}$  subunit was discussed and the full system was treated by coupling coarse-grained subunits. The polarized ground state could not be explained because all the 3 exchange integrals turned out to be antiferromagnetic, but it was speculated that it should arise for longer-ranged ferromagnetic interactions. The approach was refined in a pivotal follow-up work [15], where the first 7 exchange integrals were computed, and  $J_5$  turned out to be ferromagnetic (see Fig. 1). The specific heat and the magnetization curve were computed in terms of the classical Ising and Potts models by using a geometry-adapted tensor-network representation of the partition function.

In this paper, we significantly extend these results: We show that the full Heisenberg model for  $\{\text{Mn}_{84}\}$  ( $S = 2$ )

$L$	geometry features	spin values/max. spin	$S_{\text{tot}}$	$S_{\text{tot}}/S_{\text{max}}$	Ref.
30	C <sub>2</sub> , near-octahedral	$3 \cdot 5/2 + 26 \cdot 2 + 3/2 = 61$	5-7	0.08-0.11	[4, 5]
32	mostly octahedral	$18 \cdot 5/2 + 10 \cdot 2 + 4 \cdot 3/2 = 71$	5	0.07	[6]
32	truncated cube	$24 \cdot 5/2 + 8 \cdot 3/2 = 72$	9-10	0.13-0.14	[7]
32	“double-decker wheel”	$18 \cdot 5/2 + 14 \cdot 2 = 73$	11-12	0.15-0.16	[8]
40	“loop of loops”	$8 \cdot 5/2 + 32 \cdot 2 = 84$	4	0.05	[9]
70	giant wheel	$70 \cdot 2 = 140$	5-8	0.04-0.06	[2]
84	giant wheel	$84 \cdot 2 = 164$	6	0.04	[3]

TABLE I: Selection of low-spin molecular complexes that have Mn atoms as magnetic centres.

is in fact tractable using the density-matrix renormalization group (DMRG). This means that by exploiting the full SU(2) symmetry of the problem, we are able to resolve energy gaps of  $\sim 10^{-4}J_1$ . We use the published set of exchange integrals [15], but neglect the small long-range values  $J_6$  and  $J_7$ , which complicate the numerics. We demonstrate that the remaining 5 exchange integrals [15] quantitatively reproduce the low-spin state  $S_{\text{tot}}/N_{\text{cells}} \approx 1$  without any additional fitting.

## II. TECHNICAL DETAILS

For the finite rings, we employ the *density-matrix renormalization group* (DMRG), which approximates the ground-state wavefunction as a matrix-product state (MPS), capturing entanglement and correlations through iterative optimization and state truncation. The key control parameter is the “bond dimension”  $\chi$  that corresponds to the number of variational parameters in the MPS ansatz. DMRG has proven quite effective for finite molecular systems described by the Heisenberg model [16, 17]. As a rigorous measure of accuracy, we employ the variance per site given by

$$\text{var}/L = \left| \left\langle \frac{H^2}{J_1^2} \right\rangle - \left\langle \frac{H}{J_1} \right\rangle^2 \right| / L. \quad (4)$$

We extrapolate the energy per site by a linear ansatz  $E/L = (E/L)_{\text{exact}} + \alpha \cdot \text{var}/L$  [18]. We use the two-site DMRG algorithm to grow the bond dimension for the first iterations before switching to the cheaper one-site algorithm with perturbations [19]. Periodic boundary conditions (PBC) are implemented as long-range terms on the level of the matrix-product operator (MPO) representation of the Hamiltonian, and the bandwidth of the interaction graph  $J_{ij}$  is minimized using the reverse Cuthill-McKee algorithm [16, 20].

Furthermore, the SU(2) symmetry of the model (1) with  $B = 0$  allows us to increase efficiency by working in the reduced spin basis. This means that an SU(2)-invariant bond dimension  $\chi_{\text{SU}(2)}$  corresponds to a much larger  $\chi_{\text{eff}}$ . For the  $S = 2$  system investigated here we find  $\chi_{\text{eff}} \sim 7\chi_{\text{SU}(2)}$ , i.e. almost an order-of-magnitude gain. Moreover, the exploitation of SU(2) symmetry allows us to directly target states with a given quantum number  $S_{\text{tot}}$  and compute the energy curve  $E(S_{\text{tot}})$ .

For an infinite chain, we employ the related *variational uniform matrix-product state* (VUMPS) formalism [21]. As a state error which is analogous to Eq. (4), we employ the two-site variance defined in Ref. [21]. By varying the exploited symmetry, we can perform a cross-diagnostic analysis: (i) If the full SU(2) symmetry is exploited, we can only look at the  $S_{\text{tot}} = 0$  case with unbroken symmetry. For a bipartite system with equal spin values, this would be the ground state by the Lieb-Mattis theorem [22], but the theorem is not valid in the case of frustration. (ii) If the U(1) symmetry is exploited, we can compare different rational polarizations within the numerical unit cell. (iii) If no symmetry is exploited, DMRG tends to converge to the lowly entangled sector with  $M_{\text{tot}}/L = S_{\text{tot}}/L$  and we can directly compute the total spin per site [18], which might be irrational. We take the numerical unit cell to be equal to the Mn<sub>14</sub> subunit. We use meV as the energy scale throughout the work.

## III. INFINITE NUMBER OF UNIT CELLS

As a guiding principle for  $\{\text{Mn}_{84}\}$ , we first look at an infinite number of unit cells in the ideal case of the thermodynamic limit. Figure 2 shows the results obtained by VUMPS. We converge the state for various bond dimensions, and plot the resulting energies as a function of the state error defined in Ref. [21]. The lowest energy is in fact achieved without symmetries having a polarization of  $M_{\text{tot}}/N_{\text{cells}} \approx 0.96$ . The energy is very close to the rational case of  $M_{\text{tot}}/N_{\text{cells}} = 1$  with U(1) symmetry. The spin singlet is also close in energy, but remains slightly above. Higher rational polarizations within the 14-site unit cell are clearly excited states. Our conclusion is that the system prefers a state with an irrational polarization close to, but not exactly equal to  $M_{\text{tot}}/N_{\text{cells}} = 1$ , with a small energy barrier towards the singlet. For finite systems up to  $L = 84$  where the total spin can only change in integer steps, we expect to have the lowest energy at the nearest integer value to  $S_{\text{tot}} \approx 0.96N_{\text{cells}}$ .

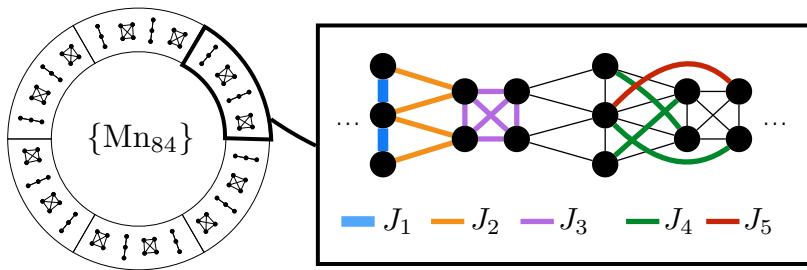


FIG. 1: Left: Schematic picture of the spin sites in  $\{\text{Mn}_{84}\}$ . Right: The 14-site unit cell of the Mn wheels, consisting out of the 3-site line piece and the 4-site tetrahedron. The first 5 DFT-calculated exchange interactions are (in units of meV):  $J_1 = 13$ ,  $J_2 = 3.2$ ,  $J_3 = 1.1$ ,  $J_4 = 0.4$ ,  $J_5 = -1.7$ . Only  $J_5$  is ferromagnetic. The couplings are periodically extended, but  $J_1$ - $J_3$  ( $J_4$ ,  $J_5$ ) are only highlighted in color within the first (second) 7-site segment.

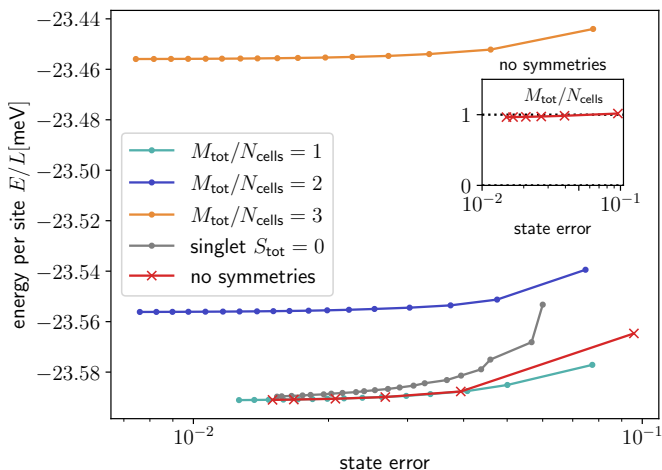


FIG. 2: The energy per site for an infinite number of coupled  $\text{Mn}_{14}$  units as a function of the state error (for the definition see [21]) for various fixed symmetries ( $B = 0$ ). The final bond dimensions reach  $\chi = 500$  (no symmetries),  $\chi \sim 2000$  [U(1)] and  $\chi_{\text{SU}(2)} \sim 3000$  [SU(2)]. The inset shows the computed spin per number of unit cells for the case without symmetries; a linear fit gives the extrapolated value of  $M_{\text{tot}}/N_{\text{cells}} \approx 0.96$ .

#### IV. FINITE RINGS

We test the infinite-system prediction on finite rings of  $N_{\text{cells}} = 2, 3, 4, 5, 6$  using PBC by computing the energy in each spin sector in the range  $S_{\text{tot}} = 0 - 8$ . This is shown in Fig. 3, which is the central result of our work.

For  $N_{\text{cells}} = 2, 3, 4$ , there is rapid convergence for  $\chi_{\text{SU}(2)} \leq 4000$ . The variance per site is of the order of  $10^{-4}$  for  $\chi_{\text{SU}(2)} = 4000$ . For  $N_{\text{cells}} = 5, 6$  (which correspond to the physical cases of  $\{\text{Mn}_{70}\}$  and  $\{\text{Mn}_{84}\}$ ), the gaps become smaller and we have to go up to  $\chi_{\text{SU}(2)} = 8000$  to obtain the same accuracy. The result in all cases is a minimum at the value  $S_{\text{tot}}/N_{\text{cells}} = 1$ . However,  $S_{\text{tot}} = 5$  and  $S_{\text{tot}} = 6$  are extremely close in energy for  $\{\text{Mn}_{84}\}$  and  $S_{\text{tot}} = 6$  only wins by a very small margin for  $\chi_{\text{SU}(2)} = 8000$ . A conservative estimate is that

$S_{\text{tot}} = 5, 6$  are near-degenerate for  $\{\text{Mn}_{84}\}$  with an energy per site of  $E/(LJ_1) = -1.8148 \pm 0.0002$ .

Overall, our large-scale DMRG calculations paired with exchange integrals from DFT are a decisive confirmation of the experimentally measured total-spin state of  $\text{Mn}_{84}$ . There may still be some influence from factors we have neglected, such as the inclusion of longer-ranged couplings or distortions in the interatomic distances. We assume that these additional influences remain small enough to preserve the general shape of the  $S_{\text{tot}}/N_{\text{cells}} \approx 1$  minimum.

#### V. DEPENDENCE ON THE SPIN QUANTUM NUMBER

We briefly test whether the low-spin minimum would appear with the same geometry and the same exchange parameters, but for a hypothetical  $S = 1$  system. Figure 4 shows the results. We see that the  $E(S_{\text{tot}})$  curves now remain convex for the finite systems with a minimum at  $S_{\text{tot}} = 0$ . The infinite-system calculation similarly shows  $M_{\text{tot}} \approx 0$ .

We conclude that for an  $S = 1$  system, the singlet ground state is robust against weak ferromagnetic perturbations, whereas it becomes susceptible to it in the case of  $S = 2$ , resulting in a polarized ground state. Intuitively, it is clear that due to a large number of internal states, a high spin can “afford” a coexistence of a partial polarization and quantum fluctuations to minimize the energy, and in this sense becomes more classical. The non-trivial result is that this transition happens between  $S = 1$  and  $S = 2$ . This may explain the multitude of low-spin Mn-based SMMs listed in Tab. I, since the Mn sites have a local spin value that varies in the range  $S = 2 \pm 0.5$  depending on the oxidation state ( $\text{Mn}^{2+}$  to  $\text{Mn}^{4+}$ ).

#### VI. MAGNETIZATION CURVE

In this section we compute the full magnetization curve for  $B > 0$ . This requires the calculation of the lowest energies for all sectors between  $S_{\text{tot}} = 0$  and  $S_{\text{tot}} = S \cdot L$ .

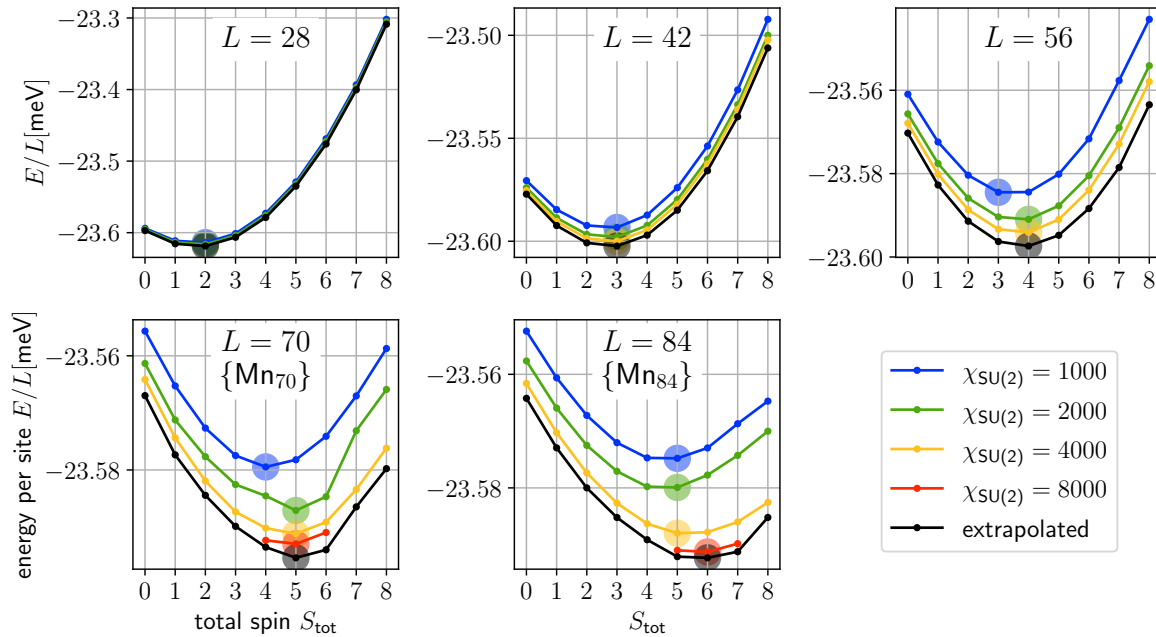


FIG. 3: Ground-state energies per site (spin) of the rings with  $N_{\text{cells}} = 2, 3, 4, 5, 6$  (corresponding to  $L = 28, 42, 56, 70, 84$ ) in the spin sectors up to  $S_{\text{tot}} = 8$  ( $B = 0$ ) for various bond dimensions  $\chi_{\text{SU}(2)}$ . The black dots are linearly extrapolated in the variance per site (see Sec. II). A circle highlights the energy minimum for each dataset. A low-spin minimum at  $S_{\text{tot}}/N_{\text{cells}} = 1$  is found for all system sizes.

For a given value of  $B$ , the correct ground-state sector with  $M = S_{\text{tot}}$  follows from minimizing

$$\begin{aligned} \min_{S_{\text{tot}}} E(B, S_{\text{tot}}) &= \min_{S_{\text{tot}}} \langle S_{\text{tot}}, M = S_{\text{tot}} | H | S_{\text{tot}}, M = S_{\text{tot}} \rangle \\ &= \langle S_{\text{tot}} | \sum_{ij} J_{ij} \mathbf{S}_i \cdot \mathbf{S}_j | S_{\text{tot}} \rangle - g\mu_B B S_{\text{tot}}. \end{aligned} \quad (5)$$

Since this is a large volume of computations, we limit ourselves to  $\chi_{\text{SU}(2)} = 1000$ . However, the full spectrum is on an energy scale of  $> 4500\text{meV}$ , so that sub-meV energy inaccuracies carry no weight in this case. Moreover, the reduced Hilbert space at high spins makes the calculations easier and we find that all the energies with  $S_{\text{tot}} \gtrsim 114$  for  $L = 84$  are in fact numerically exact for this bond dimension.

The result is shown in Fig. 5. We see a linear increase in the magnetization (with finite-size steps) until  $g\mu_B B \sim 16\text{meV}$  (i.e. until the field becomes larger than the dominant exchange  $J_1 = 13\text{meV}$ ). This is followed by a wide plateau at  $10/14$  of the saturation, and again by three more narrow plateaus at  $11/14$ ,  $12/14$  and  $13/14$ . We note that due to the large value of  $J_1$  (which corresponds to  $T \approx 151\text{K}/k_B$ ) even the first plateau will be quite difficult to observe, requiring at least  $B \sim 160\text{T}$ .

To better understand the origin of the plateaus, we compute the site-resolved magnetizations  $\sum_i \langle S_i^z \rangle$  and find that the tetrahedra at these plateaus are almost completely polarized with  $M_{\text{tetra}} \approx 8$ . This is understandable because they are much weaker coupled with

$J_3 = 1.1\text{meV}$ . Since the line pieces are coupled via the tetrahedra (cf. Fig. 1), they disconnect and the physics should be given by an ensemble of independent 3-site clusters described by the Hamiltonian

$$H_{\text{eff}} = J(\mathbf{S}_1 \cdot \mathbf{S}_2 + \mathbf{S}_2 \cdot \mathbf{S}_3) - g\mu_B B \sum_{i=1}^3 S_i^z. \quad (6)$$

We compute the magnetization curve of  $H_{\text{eff}}$  for  $S = 2$  [see Fig. 6 b)] and find a  $2/6$  plateau of width  $g\mu_B \Delta B = 3J$ , as well as three plateaus at  $3/6$ ,  $4/6$ ,  $5/6$  of width  $g\mu_B \Delta B = J$ . The central spin aligns itself antiparallel to the others to maximize the exchange energy and is flipped in a stepwise fashion. This quantitatively corresponds to the number and widths of the plateaus for the full case in Fig. 5 by setting  $J = J_1 = 13\text{meV}$  and rescaling the fraction of the saturation by including the tetrahedra:  $M/M_{\text{sat}} = (n + 8)/(6 + 8)$  (with  $n = 2, 3, 4, 5$ ).

Magnetization plateaus are typically related to localized magnons, where spinflips localize due to a canceling of hopping terms on a frustrated geometry [23–26]. In our case, the reason for localization are the inhomogeneous interactions, whereby the external field breaks up the system into independent islands by breaking the weak bonds that connect them.

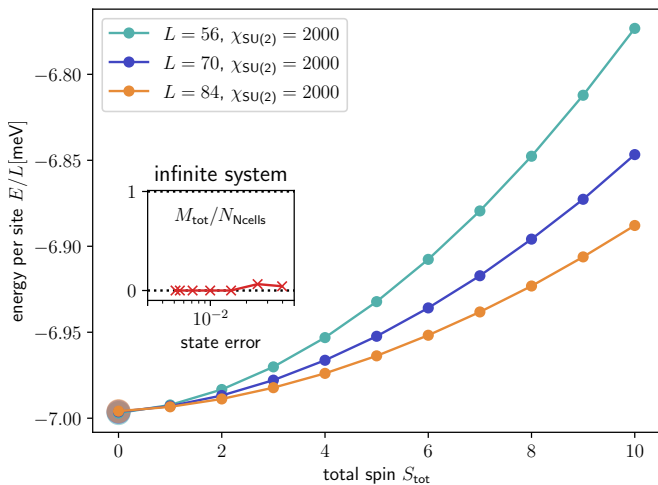


FIG. 4: Ground-state energies per site of the rings with  $N_{\text{cells}} = 4, 5, 6$  (corresponding to  $L = 56, 70, 84$ ) for a hypothetical  $S = 1$  system with the same geometry and exchange parameters as in Fig. 1. All data are for  $\chi_{\text{SU}(2)} = 2000$ , which corresponds to a variance per site of the order of  $10^{-5}$ . The inset shows the polarization of the infinite system without symmetries as a function of the state error. No low-spin minimum is found in this case.

## VII. CONCLUSION

We have studied the quantum Heisenberg model on the geometry of the Mn giant wheels using a set of DFT-computed exchange parameters [15] combined with large-scale SU(2)-symmetric DMRG calculations. The presence of a unit cell allows us to scale the system size from finite rings with  $N_{\text{cells}} = 2 - 6$ , as well as compare with the infinite chain as a guiding case. The result is a clear minimum at a total spin  $S_{\text{tot}}/N_{\text{cells}} \approx 1$ , which quantitatively reproduces the experimental values ( $S_{\text{tot}} = 6$  for  $\{\text{Mn}_{84}\}$ ,  $N_{\text{cells}} = 6$ ) without any additional free parameters. This shows that theory has caught up with experimental progress in manufacturing high-nucleation SMMs and is able to successfully describe large finite magnetic systems with  $L \sim 100$  spin sites.

By reducing the spin quantum number to  $S = 1$ , we find that the energy minimum robustly remains at  $S_{\text{tot}} = 0$ . Thus we argue that systems with  $S \gtrsim 2$  become susceptible to the presence of small ferromagnetic exchange interactions and react to them by a partial ground-state polarization. This explains the multitude of low-spin SMMs that are based on Mn ions, and marks a crossover point from quantum to classical spins.

Finally, we find magnetization plateaus at  $10/14$ ,  $11/14$ ,  $12/14$  and  $13/14$  of the saturation which are a consequence of the inhomogeneous interactions in the system. They can be explained by independent 3-site clusters whose weak inter-cluster couplings are broken by the

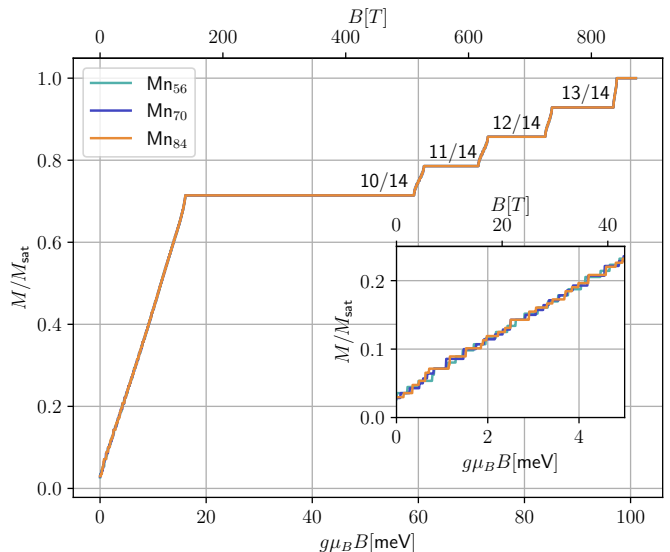


FIG. 5: Magnetization curve for  $L = 56, 70, 84$ , obtained by computing the energies in all spin sectors  $S_{\text{tot}} = 0$  to  $S_{\text{tot}} = S \cdot L = 2L$  with  $\chi_{\text{SU}(2)} = 1000$ . The curves are practically on top of each other on this scale. The inset shows a zoom-in on the low-field onset.

external field.

## Acknowledgements

C.K. and R.R. acknowledge support by the Deutsche Forschungsgemeinschaft (DFG, German Research Foundation) under Germany's Excellence Strategy EXC-2123 QuantumFrontiers 390837967.

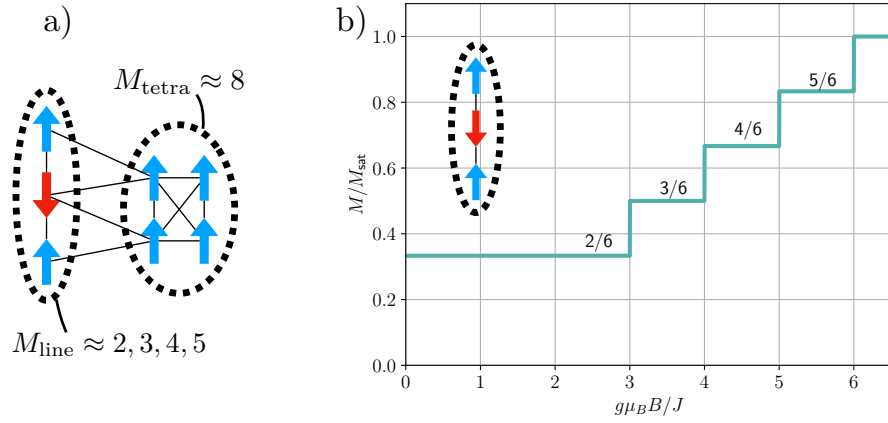


FIG. 6: a) Schematic representation of the local polarization at the magnetization plateaus. The 10/14, 11/14, 12/14, 13/14 plateaus correspond to magnetization values of the line piece of  $M_{\text{line}} = 2, 3, 4, 5$ , while the tetrahedron is nearly fully polarized. b) Magnetization curve of a 3-spin line piece with  $S = 2$ .

- [1] C. Papatriantafyllopoulou, E. E. Moushi, G. Christou, and A. J. Tasiopoulos, Filling the gap between the quantum and classical worlds of nanoscale magnetism: giant molecular aggregates based on paramagnetic 3d metal ions, *Chem. Soc. Rev.* **45**, 1597 (2016).
- [2] A. Vinslava, A. J. Tasiopoulos, W. Wernsdorfer, K. A. Abboud, and G. Christou, Molecules at the quantum-classical nanoparticle interface: Giant  $\text{Mn}_{70}$  single-molecule magnets of  $\sim 4$  nm diameter, *Inorganic Chemistry* **55**, 3419 (2016).
- [3] A. J. Tasiopoulos, A. Vinslava, W. Wernsdorfer, K. A. Abboud, and G. Christou, Giant single-molecule magnets: A  $\text{Mn}_{84}$  torus and its supramolecular nanotubes, *Angewandte Chemie International Edition* **43**, 2117 (2004), <https://onlinelibrary.wiley.com/doi/pdf/10.1002/anie.200353350>.
- [4] M. Soler, E. Rumberger, K. Folting, D. N. Hendrickson\*, and G. Christou\*, Synthesis, characterization and magnetic properties of  $[\text{mn}_3\text{o}_24(\text{oh})_8(\text{o}_2\text{cch}_2\text{c}(\text{ch}_3)_3)_32(\text{h}_2\text{o})_2(\text{ch}_3\text{no}_2)_4]$ : the largest manganese carboxylate cluster, *Polyhedron* **20**, 1365 (2001).
- [5] M. Soler, W. Wernsdorfer, K. Folting, M. Pink, and G. Christou, Single-molecule magnets: a large  $\text{Mn}_{30}$  molecular nanomagnet exhibiting quantum tunneling of magnetization, *Journal of the American Chemical Society* **126**, 2156 (2004).
- [6] S. K. Langley, R. A. Stott, N. F. Chilton, B. Moubaraki, and K. S. Murray, A high nuclearity mixed valence  $\text{Mn}_{32}$  complex, *Chem. Commun.* **47**, 6281 (2011).
- [7] R. T. W. Scott, S. Parsons, M. Murugesu, W. Wernsdorfer, G. Christou, and E. K. Brechin, Linking centered manganese triangles into larger clusters: A  $\text{Mn}_{32}$  truncated cube, *Angewandte Chemie International Edition* **44**, 6540 (2005), <https://onlinelibrary.wiley.com/doi/pdf/10.1002/anie.200501821>.
- [8] M. Manoli, R. Inglis, M. J. Manos, V. Nastopoulos, W. Wernsdorfer, E. K. Brechin, and A. J. Tasiopoulos, A  $[\text{Mn}_{32}]$  double-decker wheel, *Angewandte Chemie International Edition* **50**, 4441 (2011), <https://onlinelibrary.wiley.com/doi/pdf/10.1002/anie.201100976>.
- [9] E. E. Moushi, C. Lampropoulos, W. Wernsdorfer, V. Nastopoulos, G. Christou, and A. J. Tasiopoulos, A large  $[\text{Mn}_{10}\text{Na}]_4$  loop of four linked  $\text{Mn}_{10}$  loops, *Inorganic Chemistry* **46**, 3795 (2007).
- [10] N. Regnault, T. Jolicœur, R. Sessoli, D. Gatteschi, and M. Verdager, Exchange coupling in the magnetic molecular cluster  $\text{Mn}_{12}\text{Ac}$ , *Phys. Rev. B* **66**, 054409 (2002).
- [11] K. Park, M. R. Pederson, and C. S. Hellberg, Properties of low-lying excited manifolds in  $\text{Mn}_{12}$  acetate, *Phys. Rev. B* **69**, 014416 (2004).
- [12] G. Chaboussant, A. Sieber, S. Ochsenein, H.-U. Güdel, M. Murrie, A. Honecker, N. Fukushima, and B. Normand, Exchange interactions and high-energy spin states in  $\text{Mn}_{12}$ -acetate, *Phys. Rev. B* **70**, 104422 (2004).
- [13] R. Bagai and G. Christou, The drosophila of single-molecule magnetism:  $[\text{Mn}_{12}\text{O}_{12}(\text{O}_2\text{CR})_{16}(\text{H}_2\text{O})_4]$ , *Chem. Soc. Rev.* **38**, 1011 (2009).
- [14] H. F. Schurkus, D. Chen, M. J. O'Rourke, H.-P. Cheng, and G. K.-L. Chan, Exploring the magnetic properties of the largest single-molecule magnets, *The Journal of Physical Chemistry Letters* **11**, 3789 (2020).
- [15] D.-T. Chen, P. Helms, A. R. Hale, M. Lee, C. Li, J. Gray, G. Christou, V. S. Zapf, G. K.-L. Chan, and H.-P. Cheng, Using hyperoptimized tensor networks and first-principles electronic structure to simulate the experimental properties of the giant  $\text{Mn}_{84}$  torus, *The Journal of Physical Chemistry Letters* **13**, 2365 (2022).
- [16] R. Rausch, C. Plorin, and M. Peschke, The antiferromagnetic  $S = 1/2$  Heisenberg model on the  $\text{C}_{60}$  fullerene geometry, *SciPost Phys.* **10**, 087 (2021).
- [17] R. Rausch, M. Peschke, C. Plorin, and C. Karrasch, Magnetic properties of a capped kagome molecule with 60 quantum spins, *SciPost Phys.* **12**, 143 (2022).
- [18] R. Rausch, M. Peschke, C. Plorin, J. Schnack, and C. Karrasch, Quantum spin spiral ground state of the ferrimagnetic sawtooth chain, *SciPost Phys.* **14**, 052 (2023).
- [19] C. Hubig, I. P. McCulloch, U. Schollwöck, and F. A. Wolf, Strictly single-site dmrg algorithm with subspace expansion, *Phys. Rev. B* **91**, 155115 (2015).
- [20] J. Ummethum, J. Schnack, and A. M. Läuchli, Large-scale numerical investigations of the antiferromagnetic heisenberg icosidodecahedron, *Journal of Magnetism and Magnetic Materials* **327**, 103 (2013).
- [21] V. Zauner-Stauber, L. Vanderstraeten, M. T. Fishman, F. Verstraete, and J. Haegeman, Variational optimization algorithms for uniform matrix product states, *Phys. Rev. B* **97**, 045145 (2018).
- [22] E. Lieb and D. Mattis, Ordering energy levels of interacting spin systems, *Journal of Mathematical Physics* **3**, 749 (1962).
- [23] J. Schnack, H.-J. Schmidt, J. Richter, and J. Schulenburg, Independent magnon states on magnetic polytopes, *The European Physical Journal B - Condensed Matter and Complex Systems* **24**, 475 (2001).
- [24] J. Schulenburg, A. Honecker, J. Schnack, J. Richter, and H.-J. Schmidt, Macroscopic magnetization jumps due to independent magnons in frustrated quantum spin lattices, *Phys. Rev. Lett.* **88**, 167207 (2002).
- [25] J. Richter, J. Schulenburg, A. Honecker, J. Schnack, and H.-J. Schmidt, Exact eigenstates and macroscopic magnetization jumps in strongly frustrated spin lattices, *Journal of Physics: Condensed Matter* **16**, S779 (2004).
- [26] J. Richter, Localized-magnon states in strongly frustrated quantum spin lattices, *Low Temperature Physics* **31**, 695 (2005), [https://pubs.aip.org/aip/ltp/article-pdf/31/8/695/8233353/695\\_1\\_online.pdf](https://pubs.aip.org/aip/ltp/article-pdf/31/8/695/8233353/695_1_online.pdf).